APC/C^{FZR-1} Controls ZYG-1 Levels to Regulate Centrosome Assembly

Running title: ZYG-1 is an APC/C^{FZR-1} Substrate

Jeffrey C. Medley[1,2], Joseph R. DiPanni[1,2], Luke Schira[1], Blake M. Shaffou[1], Brandon M. Sebou[1], and Mi Hye Song[1,3]

[1]Department of Biological Sciences, Oakland University, Rochester, MI 48309, USA.

[2]These authors equally contributed to this work.

[3]To whom correspondence should be addressed.

Corresponding author: Mi Hye Song (msong2@oakland.edu)

Key words: APC/C; FZR-1; *C. elegans*; Centrosome; Proteolysis; ZYG-1

Abstract

Aberrant centrosome numbers are associated with human cancers. The levels of centrosome regulators positively correlate with centrosome number. Thus, tight control of centrosome protein levels is critical. In *Caenorhabditis elegans*, the anaphase-promoting complex/cyclosome and co-activator FZR-1 (APC/C^{FZR-1}) ubiquitin ligase negatively regulates centrosome assembly through SAS-5 degradation. In this study, we identify the *C. elegans* ZYG-1 (Plk4 in human) as a new substrate of APC/C^{FZR-1}. Inhibiting APC/C^{FZR-1} or mutating a ZYG-1 destruction (D)-box leads to elevated ZYG-1 levels at centrosomes, restoring bipolar spindles and embryonic viability to *zyg-1* mutants, suggesting that APC/C^{FZR-1} targets ZYG-1 for proteasomal degradation via D-box motif. We also show the Slimb/βTrCP-binding (SB) motif is critical for ZYG-1 degradation, substantiating a conserved mechanism by which ZYG-1/Plk4 stability is regulated by $SCF^{Slimb/βTrCP}$-dependent proteolysis via the conserved SB motif in *C. elegans*. Furthermore, inhibiting both APC/C^{FZR-1} and $SCF^{Slimb/βTrCP}$, by co-mutating ZYG-1 SB and D-box motifs, stabilizes ZYG-1 in an additive manner, conveying that APC/C^{FZR-1} and $SCF^{Slimb/βTrCP}$ ubiquitin ligases function cooperatively for timely ZYG-1 destruction in *C. elegans* embryos where ZYG-1 activity remains at threshold level to ensure normal centrosome number.

Introduction

Centrosomes, as the primary microtubule-organizing centers, establish bipolar mitotic spindles that ensure accurate transmission of genomic content into two daughter cells. To sustain genomic integrity, centrosome number must be strictly controlled by duplicating only once per cell cycle. Abundance of centrosome factors directly influences centrosome number. Blocking degradation of centrosome factors causes extra centrosomes, while their depletion inhibits centrosome duplication (Nigg and Holland, 2018). The ubiquitin-proteasome system provides a key mechanism to control centrosome protein levels (Nakayama and Nakayama, 2006). Levels of core centrosome factors are shown to be regulated by proteasomal degradation through E3 ubiquitin ligases, including the Anaphase Promoting Complex/Cyclosome (APC/C) and the SKP1-CUL1-F-box-protein (SCF), and their regulatory mechanisms appear to be conserved (Arquint et al., 2012; Cunha-Ferreira et al., 2009; Guderian et al., 2010; Holland et al., 2010; Medley et al., 2017a; Meghini et al., 2016; Peel et al., 2012; Puklowski et al., 2011; Rogers et al., 2009; Strnad et al., 2007; Tang et al., 2009). In *C. elegans*, the kinase ZYG-1 is a key centrosome regulator and ZYG-1 levels are critical for normal centrosome number and function (O'Connell et al., 2001; Song et al., 2008). Abundance of Plk4 (human homolog of ZYG-1) is regulated by the SCF-mediated proteasomal degradation through the F-box protein Slimb/βTrCP (*Drosophila*/humans) (Cunha-Ferreira et al., 2009; Holland et al., 2010; Rogers et al., 2009). Such mechanism is conserved in *C. elegans* where ZYG-1 levels are controlled by the $SCF^{Slimb/\beta TrCP}$ dependent proteolysis (Peel et al., 2012). While $SCF^{Slimb/\beta TrCP}$-dependent proteolysis of Plk4/ZYG-1 is well-established, additional mechanisms for control of Plk4/ZYG-1 levels have also been implicated (Cajanek et al., 2015; Holland et al., 2010; Klebba et al., 2013; Peel et al. 2012). Another E3 ubiquitin ligase, APC/C, also regulates levels of centrosome factors. In *C. elegans*, FZR-1 (Cdh1 in human), a coactivator of APC/C, negatively influences centrosome assembly, and APC/C^{FZR-1}-dependent proteolysis regulates SAS-5 levels through a

KEN-box motif (Kemp et al., 2007; Medley et al., 2017a), which is conserved in humans and flies where APC/C$^{Cdh1/Fzr}$ targets core centrosome factors (human STIL/SAS-5, SAS-6, CPAP/SAS-4 and *Drosophila* Spd2) via KEN-box (Arquint and Nigg, 2014; Meghini et al., 2016; Strnad et al., 2007; Tang et al., 2009). In this study, we investigated ZYG-1 as a potential substrate of APC/C^{FZR-1}, and how two E3 ubiquitin ligases APC/C^{FZR-1} and SCF$^{Slimb/\beta TrCP}$ influence ZYG-1 levels in centrosome assembly.

Results and Discussion

Loss of FZR-1 leads to Elevated ZYG-1 Levels at Centrosomes

Prior study identified SAS-5 as a substrate of APC/C^{FZR-1}, and implicated that APC/C^{FZR-1} might target additional centrosome regulators in *C. elegans* embryos (Medley et al., 2017a). The APC/C coactivator, FZR-1, was identified as a genetic suppressor of ZYG-1 since loss of *fzr-1* restores embryonic viability and centrosome duplication to the *zyg-1(it25)* mutant (Kemp et al., 2007; Medley et al., 2017a). Given the strong genetic interaction between *zyg-1* and *fzr-1,* a compelling possibility is that ZYG-1 might be a substrate of APC/C^{FZR-1}. In *C. elegans* embryos, while cellular ZYG-1 protein remains low throughout the cell cycle, centrosome-associated ZYG-1 is regulated during the cell cycle, peaking at anaphase and declining toward mitotic exit (Song et al., 2008, 2011).

If ZYG-1 is degraded by the APC/C^{FZR-1}-mediated proteolysis, inhibiting APC/C^{FZR-1} should protect ZYG-1 from destruction leading to protein accumulation. To address this, we stained embryos with anti-ZYG-1 and quantified fluorescence intensity of centrosome-associated ZYG-1 signal (**Fig. 1**). Quantitative immunofluorescence (IF) reveal that, compared to the wild-type (WT) control (1.00 ± 0.25 fold), *fzr-1* mutant embryos exhibit increased levels of centrosomal ZYG-1 during the first anaphase (1.28 ± 0.27 fold). *zyg-1(it25)* contains a temperature-sensitive (ts) point mutation (P442L) within the cryptic polo-box (CPB) domain that is critical for centrosomal localization of ZYG-1 (Fig 2A) (Kemphues et al., 1988; O'Connell et

al., 2001; Shimanovskaya et al., 2014). In *zyg-1(it25)* embryos, centrosomal ZYG-1 is reduced to ~40% of the WT control. By contrast, ZYG-1 levels in *zyg-1(it25) fzr-1(bs31)* double-mutant centrosomes are significantly increased (0.80 ± 0.33 fold) compared to *zyg-1(it25)* mutants, indicating the *fzr-1* mutation leads to partial restoration of centrosomal ZYG-1 in *zyg-1(it25)* mutants.

Thus, loss of FZR-1 leads to increased levels of ZYG-1 at centrosomes, which should compensate for impaired ZYG-1 function and rescue the *zyg-1* mutant phenotypes observed previously (Kemp et al., 2007, Medley et al., 2017a). These results support a hypothesis that ZYG-1 levels are regulated by APC/C^{FZR-1}-dependent proteasomal degradation. Despite exhaustive efforts to address how loss of FZR-1 impacted cellular ZYG-1 levels, we were unable to detect endogenous ZYG-1 by immunoblot or immunoprecipitation (IP) due to extremely low abundance of ZYG-1. However, our IP data suggest a possible physical interaction between ZYG-1 and FZR-1 (**Fig. S1**), further supporting that ZYG-1 is a potential target of APC/C^{FZR-1}.

ZYG-1 Contains Putative Destruction (D)-box Degron Motifs

The APC/C^{FZR-1} E3 ubiquitin ligase targets specific substrates via interaction of the coactivator FZR-1 with conserved motifs, predominantly the destruction (D)-box and KEN-box degrons, within the substrate (Glotzer et al., 1991; Pfleger and Kirschner, 2000). While ZYG-1 does not contain a KEN-box, in silico analysis identified four putative D-box motifs (RxxL) within ZYG-1. We thus asked if APC/C^{FZR-1} might target ZYG-1 for proteasomal degradation through D-box motif. In the ZYG-1 protein structure (**Fig. 2A**), D-box1 motif resides within the kinase domain and D-box4 inside of the CPB domain, D-box2 at the center of the Linker 1 (L1) domain, and D-box3 at the junction between the L1 and CPB domain (Lettman et al., 2013; O'Connell et al., 2001; Shimanovskaya et al., 2014). The sequence alignments illustrate that D-box1 is the only conserved motif in the closely related nematodes (**Fig. S2**). Structural study on the D-box and

APC/C binding shows that R-residue of D-box (RxxL) motif interacts with acidic residues of Cdh1 and L-residue is anchored into the hydrophobic pocket of Cdh1, indicating two critical residues for the Cdh1/FZR-1 interaction with substrate (He et al., 2013).

To determine if any of four putative D-boxes might be functional degron, we mutated each D-box (RxxL) by substituting two critical residues to alanine (AxxA) in wild-type(N2) animals (**Fig. 2A**). By using CRISPR/Cas9 genome editing, we generated D-box2 and D-box3 mutants with two-alanine substitution (2A; AxxA), termed the ZYG-1:DB2(2A) and ZYG-1:DB3(2A) mutation. However, the 2A mutation of D-box1 or D-box4 motif produced sterile hermaphrodites. Thus, we modified our strategy to obtain fertile homozygous mutants. In human cells, L45 residue within Cyclin B1 D-box motif (42RxxL45) is critical for Cyclin B1 destruction (Matsusaka et al., 2014). Referring to this, we generated D-box1 and D-box4 mutants with single-alanine substitution (1A; RxxA), termed the ZYG-1:DB1(1A) and ZYG-1:DB4(1A) mutation. All four ZYG-1 D-box mutations in the WT background produce viable progeny (**Table 1**).

Mutating ZYG-1 D-box3 Motif Leads to the *zyg-1* Suppression and Elevated Centrosomal ZYG-1

Next, we utilized the hypomorphic *zyg-1(it25)* genetic background to test how each D-box mutation affected ZYG-1 function. In *zyg-1(it25ts*) mutants, centrosome duplication fails during the first cell cycle, resulting in monopolar spindles during the second mitosis and 100% embryonic lethality at the restrictive temperature 24°C (O'Connell et al., 2001). If APC/C^{FZR-1} targets ZYG-1 through D-box motif, mutating functional D-box degron should inhibit APC/C^{FZR-1} binding, thereby protecting ZYG-1 from proteasomal destruction. ZYG-1 accumulation should then compensate for impaired ZYG-1 function in *zyg-1(it25)* mutants. By introducing the same D-box mutations in the *zyg-1(it25)* background, we asked if any D-box mutation rescued *zyg-1(it25)* mutant phenotypes. Intriguingly, the ZYG-1:DB3(2A) mutation leads to significant

restoration of embryonic viability and bipolar spindles to *zyg-1* mutants by >6-fold increase, compared to the control (**Fig. 2B,C**, **Table 1**). Notably, the ZYG-1:DB3(2A) mutation restores embryonic viability more robustly at the semi-restrictive condition (22.5°C) compared to the restrictive temperature (24°C), suggesting that the ZYG-1:DB3(2A) mutation requires ZYG-1 activity for the *zyg-1* suppression (**Table 1**).

However, the other D-box mutations further increased embryonic lethality and monopolar spindles to *zyg-1(it25)* mutants (**Fig. 2B,C, Table 1**). It appears that the *zyg-1(it25)* mutation (P442L) within the CPB domain provides a sensitized genetic environment for the ZYG-1:DB1(1A), DB2(2A) and DB4(1A) mutations, since the same D-box mutations in WT background have minor effect on embryonic survival (**Fig. 2B**, **Table1**). Therefore, ZYG-1 function might be impaired by alanine substitution at these sites, implicating that these residues are important for ZYG-1 function, presumably as part of the functional domain (discussed in **Fig. S2**; Lettman et al., 2013; O'Connell et al., 2001; Shimanovskaya et al., 2014). Although we cannot exclude the possibility that the other D-box motifs act as functional degrons, our data show mutating D-box3 motif leads to significant restoration of embryonic viability and bipolar spindles to *zyg-1* mutants (**Fig. 2B,C**), supporting a model that the ZYG-1 D-box3 motif is a functional degron that mediates the interaction of APC/C coactivator FZR-1 with ZYG-1 for proteasomal degradation.

Then, the ZYG-1:DB3(2A) mutation should inhibit APC/C$^{FZR\text{-}1}$-mediated proteolysis of ZYG-1, leading to hyperstabilization of ZYG-1. To test whether the ZYG-1:DB3(2A) mutation affected ZYG-1 stability, we examined centrosome-associated ZYG-1 by quantitative IF (**Fig. 2D**). Consistent with the *zyg-1* suppression, the ZYG-1:DB3(2A) mutation leads to elevated centrosomal ZYG-1 levels (1.48 ± 0.4 fold) compared to the *zyg-1(it25)* control (1.00 ± 0.32 fold), while the ZYG-1:DB2(2A) mutation results in a modest decrease in centrosomal ZYG-1 (0.87 ± 0.28 fold). These data suggest the ZYG-1:DB3(2A) mutation renders ZYG-1 resistant to

degradation. Although, without quantitative immunoblot data to address cellular ZYG-1 levels, it remains unclear whether APC/C^{FZR-1} regulates cellular ZYG-1 levels or affects centrosomal ZYG-1 locally, we favor a model where elevated centrosomal ZYG-1 is a direct consequence of increased cellular ZYG-1 levels (Decker et al., 2011; Song et al., 2008). Such correlation between cellular and centrosomal levels of Plk4 has been observed (Guderian et al., 2010).

Since the D-box (1A) mutation may not completely disrupt APC/C^{FZR-1} binding, it remains possible that D-box1 and 4 motifs are functional degrons. To address this, we mutated L352 of the D-box3 (349RxxL352) motif to alanine termed ZYG-1:DB3(1A) (**Fig. 2A**), and examined its consequences in *zyg-1(it25)* mutants (**Fig. S3**). The ZYG-1:DB3(1A) mutation produces neither change on centrosomal ZYG-1 nor rescue of *zyg-1(it25)* embryonic lethality, indicating both R and L residues in the ZYG-1 D-box3 (RxxL) are required for optimal APC^{FZR-1} binding and ZYG-1 destruction, unlike human Cyclin B1 (Matsusaka et al., 2014). Interestingly, the ZYG-1:DB1(1A) or DB4(1A) mutation leads to decreased centrosomal ZYG-1, suggesting that alanine substitution at these sites negatively impacted centrosomal ZYG-1 localization (**Fig. S3**). While we cannot exclude the role of D-box1 and 4 motifs as functional degrons in this study, our collective results support a model that the APC/C^{FZR-1} E3 ubiquitin ligase targets ZYG-1 for proteasomal destruction through recognition of the D-box3 motif.

ZYG-1:DB3(2A) Mutation Influences Downstream Effectors of ZYG-1

Increased centrosomal ZYG-1 by the ZYG-1:DB3(2A) mutation closely correlates with suppression of *zyg-1(it25)* phenotypes. The *zyg-1(it25)* embryo exhibits drastically reduced levels of centrosomal ZYG-1, which negatively affects the recruitment of downstream centrosome factors. ZYG-1 is required for SAS-5 and SAS-6 loading to centrosomes, then SAS-5 and SAS-6 together recruit SAS-4 (Delattre et al., 2006; Lettman et al., 2013; Pelletier et al., 2006). Later, SAS-7 was identified as centrosome factor critical for centrosomal targeting of SPD-2, and both SAS-7 and SPD-2 act upstream of ZYG-1 (Sugioka et al., 2017).

Elevated centrosomal ZYG-1 by the ZYG-1:DB3(2A) mutation should restore the recruitment of downstream centrosome factors, rendering centrosomes competent to assemble new centrioles. To test this, we quantified centrosome-associated protein levels in D-box mutants. To facilitate quantification, we generated epitope-tagged SAS-5::V5 and Ollas::SAS-6 strains using CRISPR/Cas9 genome editing (**Fig. S4**). By co-staining embryos with anti-V5 and anti-SAS-4, we first quantified fluorescence intensity of SAS-5::V5 and SAS-4 signals at centrosomes, using SAS-4 as unambiguous centrosome marker (**Fig. 2E**). At the first anaphase, the ZYG-1:DB3(2A) mutation leads to elevated centrosomal SAS-5 (1.26 ± 0.39 fold) compared to the WT control (1.00 ± 0.27), nearly equivalent to the increase in the SAS-5:KEN(3A) mutant (1.26 ± 0.37 fold; Medley et al., 2017a), whereas SAS-5 levels are decreased in the ZYG-1:DB2(2A) mutant centrosomes (0.70 ± 0.19 fold). Similarly, SAS-4 levels are increased in the ZYG-1:DB3(2A) (1.18 ± 0.22 fold) and SAS-5:KEN(3A) (1.14 ± 0.17 fold) mutant centrosomes, but reduced in the ZYG-1:DB2(2A) mutant (0.79 ± 0.22 fold). Furthermore, D-box mutations produce similar effects on SAS-5 and SAS-4 levels in *zyg-1(it25)* mutants **(Fig. S5A,C).** Since APC/C^{FZR-1} is active during late mitosis, SAS-5 and SAS-4 levels are unaffected at metaphase (**Fig. S5B,D).** Next, we examined SAS-6 levels in ZYG-1 D-box(2A) mutants expressing Ollas::SAS-6 (**Fig. 2F).** At anaphase, the ZYG-1:DB3(2A) mutation leads to increased centrosomal SAS-6 (1.26 ± 0.23 fold) compared to the WT control (1.00 ± 0.19 fold), comparable to the change in the SAS-5:KEN(3A) mutant (1.22 ± 0.23 fold), whereas the ZYG-1:DB2(2A) mutation has little effect on SAS-6 (0.94 ± 0.13 fold). Finally, we monitored dynamic changes of centrosomal GFP::SAS-7 by live imaging (**Fig. S5E**). Given SAS-7 acting upstream of ZYG-1, centrosomal SAS-7 levels are unaffected in ZYG-1 D-box mutants throughout the cell cycle. Together, our data show the ZYG-1:DB3(2A) mutation leads to elevated centrosomal ZYG-1, which promotes centrosomal loading of downstream factors, thereby restoring centrosome duplication and viability to *zyg-1* mutants.

ZYG-1 D-box3 Mutation Produces Less Robust Impact than Loss of FZR-1

While the ZYG-1:DB3(2A) mutation leads to elevated centrosomal ZYG-1, it is evident that the *fzr-1* mutation produces greater impact on ZYG-1 levels (1.86 ± 0.44 fold) than the ZYG-1:DB3(2A) mutation (**Fig. 2D**). Similar trends between *fzr-1(bs31)* and ZYG-1:DB3(2A) mutations are observed for the *zyg-1* suppression (**Fig. 2B,C**, **Table 1**).

Since the *C. elegans* SAS-5 is an APC/C^{FZR-1} substrate and mutating the SAS-5:KEN-box leads to the *zyg-1* suppression (Medley et al., 2017a), we asked if mutating the ZYG-1:D-box3 and SAS-5:KEN-box degrons simultaneously produces the effects comparable to those resulting from the *fzr-1* mutation. Instead, mutating both ZYG-1 and SAS-5 degrons leads to the *zyg-1* suppression at a level nearly equivalent to the ZYG-1:DB3(2A) mutation alone (**Fig. 2B,C, Table 1**). Consistently, the effects on centrosomal ZYG-1 levels are comparable between the ZYG-1:DB3(2A); SAS-5:KEN(3A) double mutation (1.55 ± 0.42 fold) and ZYG-1:DB3(2A) single mutation (1.48 ± 0.42 fold; **Fig. 2D**). Since SAS-5 acts downstream of ZYG-1, mutating SAS-5 KEN-box does not affect centrosomal ZYG-1 (1.02 ± 0.3 fold) while it increases SAS-5 levels (**Fig. 2D,E**; Medley et al., 2017a).

Our data illustrate the epistatic relationship between *zyg-1* and *sas-5* in centrosome assembly. Co-mutating ZYG-1 and SAS-5 degrons produces the impacts that are comparable to the ZYG-1:DB3(2A) single mutation and less potent than the *fzr-1* mutation. Thus, our results suggest that APC/C^{FZR-1} might target additional centrosome factors, likely acting upstream of ZYG-1, that support the *zyg-1* suppression. An intriguing candidate might be SPD-2 that promotes centrosomal targeting of ZYG-1 (Shimanovskaya et al., 2014). In support of this, *C. elegans* SPD-2 contains several putative D-boxes and *Drosophila* Spd2 is a known APC/C$^{Fzr/FZR-1}$ substrate (Meghini et al., 2016).

The Conserved Slimb-binding Motif is Critical for Controlling ZYG-1 Levels

While our data suggest APC/C^{FZR-1} controls ZYG-1 stability via the D-box3 motif, mutating D-box3 alone produces a modest effect on ZYG-1 levels (**Fig. 2D**), indicating that ZYG-1 is still degraded when D-box3 is mutated. These results raise the possibility that ZYG-1 levels are regulated via additional degrons (multiple D-boxes or non-canonical degrons) recognized by APC/C, or by other proteolytic pathways. Indeed, ZYG-1 levels are shown to be regulated by SCF$^{Slimb/\beta TrCP}$-mediated proteolysis (Peel et al., 2012), the mechanism of which is highly conserved (Cunha-Ferreira et al., 2009; Holland et al., 2010; Rogers et al., 2009). In *Drosophila* and human cells, the SCF$^{Slimb/\beta TrCP}$ E3 ubiquitin ligase controls Plk4 abundance through the conserved Slimb/βTrCP-binding motif (D**S**Gxx**S/T**) within Plk4, and autophosphorylation of this motif is critical for SCF$^{Slimb/\beta TrCP}$ binding and Plk4 degradation (Cunha-Ferreira et al., 2013; Guderian et al., 2010; Klebba et al., 2013).

In *C. elegans*, while inhibiting LIN-23 (Slimb/βTrCP homolog) stabilizes ZYG-1, a direct involvement of the ZYG-1:Slimb/βTrCP-binding (SB) motif (334D**S**Gxx**T**339) in ZYG-1 stability remains unclear (Peel et al., 2012). We thus asked whether the ZYG-1:SB motif influences SCF$^{Slimb/\beta TrCP}$-mediated degradation of ZYG-1. Toward this, we generated *zyg-1(it25)* mutant strains carrying alanine-substitution mutations for two critical residues within the ZYG-1:SB motif (**Fig. 3A**), equivalent to the known phosphosites (D**S**Gxx**T**) of the SB motif in Plk4 (Cunha-Ferreira et al., 2013; Guderian et al., 2010; Holland et al., 2010; Klebba et al., 2013). Single-alanine substitution mutation (S335A or T339A) leads to ~3-fold increased embryonic viability in *zyg-1(it25)* mutants compared to the control at 22.5°C (**Fig. 3B**, Table 1). Intriguingly, mutating both residues (334D**A**Gxx**A**339), termed the ZYG-1:SB(2A) mutation, restores embryonic viability to *zyg-1(it25)* mutants by >10-fold higher than the control (**Fig. 3A,B, Table 1**). Thus, both S335 and T339 residues in the ZYG-1:SB motif are critical for ZYG-1 degradation, supporting a model that SCF$^{Slimb/\beta TrCP}$ targets ZYG-1 for proteasomal degradation through the

ZYG-1:SB motif. Our data substantiate the conserved mechanism by which Plk4/ZYG-1 levels are regulated by $SCF^{Slimb/\beta TrCP}$-mediated proteolysis through the SB motif.

APC/C^{FZR-1} and $SCF^{Slimb/\beta TrCP}$ E3 Ubiquitin Ligases Regulate ZYG-1 Levels Cooperatively

Given that both APC/C^{FZR-1} and $SCF^{Slimb/\beta TrCP}$ regulate ZYG-1 levels, we asked if co-mutating ZYG-1:SB and DB3 motifs could enhance ZYG-1 protection from degradation, and produced the strain carrying double-mutation of ZYG-1:SB and DB3 motifs, termed ZYG-1:SB+DB3(4A) (**Fig. 3A**). The ZYG-1:SB (334DSGxxT339) and DB3 (349RxxL352) motifs reside in close proximity within the L1 domain (**Fig. 3A**). Whereas neither motif is conserved in closely related nematodes (**Fig. S2D**), the flanking region of these motifs appears to be somewhat conserved (Fig. 2D in Klebba et al., 2013).

In the *zyg-1(it25)* background, mutating both ZYG-1:SB and DB3 motifs further increases embryonic viability and bipolar spindles, compared to SB(2A) or DB3(2A) single mutation (**Fig. 3B,C, Table 1**). Consistently, mutating both degrons leads to further elevated centrosomal ZYG-1 levels (1.52 ± 0.37 fold) than SB (1.20 ± 0.31 fold) or DB3 (1.29 ± 0.34 fold) single mutation (**Fig. 3D**). Thus, inhibiting both APC/C^{FZR-1} and $SCF^{Slimb/\beta TrCP}$ ubiquitin ligases enhances ZYG-1 stability in an additive manner, suggesting that APC/C^{FZR-1} and $SCF^{Slimb/\beta TrCP}$-mediated proteolytic regulation cooperatively controls ZYG-1 stability via the conserved motifs.

In summary, our study reports, for the first time, that ZYG-1 levels are regulated by the APC/C^{FZR-1}-dependent proteolysis through D-box motif. Our data also support that two E3 ubiquitin ligases, APC/C^{FZR-1} and $SCF^{Slimb/\beta TrCP}$, cooperate to facilitate timely degradation of ZYG-1 during the rapid cell cycle in *C. elegans* embryos, which ensures that ZYG-1 levels remain under a critical threshold level, thereby preventing aberrant centrosome numbers (**Fig. S6**). Furthermore, our work suggests that APC/C^{FZR-1} might target additional centrosome factors

that act upstream or parallel of ZYG-1 to support the *zyg-1* suppression cooperatively. Additional work is required to further understand the regulatory mechanisms of APC/C^{FZR-1} in centrosome assembly. It will be also interesting to explore the role of APC/$C^{Cdh1/FZR-1}$ in regulating human Plk4 stability and its association with human cancers.

Methods and Materials

C. elegans Culture and Genetic Analysis

The *C. elegans* strains used in this study are listed in Table S1. All strains were derived from the wild-type Bristol N2 strain (Brenner, 1974, Church et al., 1995) and maintained on MYOB plates seeded with Escherichia coli OP50 at 16 or 19°C. For genetic analysis, individual L4 hermaphrodites were transferred to new plates and allowed to produce progeny for 24-48 h at the temperatures indicated. Progeny were allowed to develop for 18-24 h before counting the number of larvae and dead eggs.

Immunofluorescence and Cytological analysis

Immunofluorescence and confocal microscopy were performed as described (Song et al., 2008). The following primary and secondary antibodies were used at 1:3000 dilutions: DM1a (Sigma, #T9026), α-ZYG-1 (Stubenvoll et al., 2016), α-SAS-4 (Song et al., 2008), α- Myc (ThermoFisher, #PA1-981; **Fig. S4A**), and α-V5 (MBL, #M167-3; **Fig. S4B**), α-Ollas (ThermoFisher, #MA5-16125; **Fig. S4C**), Alexa Fluor 488 and 568 secondary antibodies (ThermoFisher, #A11001, A11004, A11006, A11034, A11036). Confocal microscopy was performed (Medley et al., 2017b) using a Nikon Eclipse Ti-U microscope equipped with a Plan Apo 60×1.4 NA lens, a Spinning Disk Confocal (CSU X1) and a Photometrics Evolve 512 camera. MetaMorph software (Molecular Devices, Sunnyvale, CA, USA) was used for image acquisition and quantification of the fluorescence intensity, and Adobe Photoshop/Illustrator 2020 for image processing. To quantify centrosomal signals, the average intensity within 8 or 9-

pixel (1 pixel=0.151 µm) diameter region was recorded for the highest intensity of the focal plane within an area centered on the centrosome. The average intensity within a 25-pixel diameter region drawn outside of the embryo was used for background subtraction.

CRISPR/Cas9 Genome Editing

For genome editing, we used the co-CRISPR technique described previously (Arribere et al., 2014, Paix et al., 2015). crRNA was designed using the CRISPOR web server (crispor.tefor.net; Concordet and Haeussler, 2018). Animals were microinjected with a mixture of commercially available SpCas9 (IDT, Coralville, IA) and custom-designed oligonucleotides (**Table S2,S3**) including crRNAs at 0.4–0.8 mg/ml, tracrRNA at 12 mg/ml, and single-stranded DNA oligonucleotides at 25–100 ng/ml. The amount of crRNA was tripled for low-efficiency crRNAs (ZYG-:D-box1 and D-box4, Ollas::FZR-1). After injection, we screened for *dpy-10(cn64) II/+* rollers in F1 progeny and genotyping F2. The genome editing is verified by Sanger Sequencing (GeneWiz, South Plainfield, NJ).

Statistical analysis

Statistics were produced using R statistical software and presented as average ± standard deviation (SD). Dotplots were generated using the R 'beeswarm' package. In the dotplots, box ranges from the first through third quartile of the data. Thick bar indicates the median. Solid grey line extends 1.5 times the inter-quartile range or to the minimum and maximum data point. All P-values were calculated using two-tailed t-tests: $^{ns}p>0.05$, $^{*}p<0.05$, $^{**}p<0.01$, $^{***}p<0.001$.

Acknowledgements

We thank members of Song lab (Evan Sawula and Rachel Kraft) for their technical support, Kevin O'Connell for the strains, WormBase and the *Caenorhabditis* Genetics Center (CGC). Some strains were provided by the CGC, which is funded by NIH Office of Research Infrastructure Programs (P40 OD010440).

Competing Interests

No competing interests declared.

Author Contributions

J.C.M. J.R.D. and M.H.S. designed the experiments and wrote the manuscript. J.C.M., J.R.D. and M.H.S. performed confocal imaging and data analyses. J.C.M., J.R.D., L.S., B.M.S., B.M.S. and M.H.S. performed experiments and provided data.

Funding

This work was supported by a grant (1R15GM128110-01 to M.H.S.) from the National Institute of General Medical Sciences. The funders had no role in study design, data collection and analysis, decision to publish, or preparation of the manuscript.

References

Arquint, C., and E.A. Nigg.(2014). STIL microcephaly mutations interfere with APC/C-mediated degradation and cause centriole amplification. *Curr Biol*. **24**:351-360.

Arquint, C., K.F. Sonnen, Y.D. Stierhof, and E.A. Nigg.(2012). Cell-cycle-regulated expression of STIL controls centriole number in human cells. *J Cell Sci*. **125**:1342-1352.

Arribere, J.A., R.T. Bell, B.X. Fu, K.L. Artiles, P.S. Hartman, and A.Z. Fire. (2014).Efficient marker-free recovery of custom genetic modifications with CRISPR/Cas9 in Caenorhabditis elegans. Genetics. **198**:837-846.

Brenner, S.(1974). The genetics of Caenorhabditis elegans. Genetics. 77:71-94.

Cajanek, L., T. Glatter, and E.A. Nigg.(2015). The E3 ubiquitin ligase Mib1 regulates Plk4 and centriole biogenesis. *J Cell Sci*. **128**:1674-1682.

Church, D.L., K.L. Guan, and E.J. Lambie.(1995). Three genes of the MAP kinase cascade, mek-2, mpk-1/sur-1 and let-60 ras, are required for meiotic cell cycle progression in Caenorhabditis elegans. *Development*. **121**:2525-2535.

Concordet, J.P., and M. Haeussler.(2018). CRISPOR: intuitive guide selection for CRISPR/Cas9 genome editing experiments and screens. *Nucleic Acids Res*. **46**:W242-W245.

Cunha-Ferreira, I., I. Bento, A. Pimenta-Marques, S.C. Jana, M. Lince-Faria, P. Duarte, J. Borrego-Pinto, S. Gilberto, T. Amado, D. Brito, A. Rodrigues-Martins, J. Debski, N. Dzhindzhev, and M. Bettencourt-Dias.(2013). Regulation of autophosphorylation controls PLK4 self-destruction and centriole number. *Curr Biol*. **23**:2245-2254.

Cunha-Ferreira, I., A. Rodrigues-Martins, I. Bento, M. Riparbelli, W. Zhang, E. Laue, G. Callaini, D.M. Glover, and M. Bettencourt-Dias.(2009). The SCF/Slimb ubiquitin ligase limits centrosome amplification through degradation of SAK/PLK4. *Curr Biol*. **19**:43-49.

Decker, M., S. Jaensch, A. Pozniakovsky, A. Zinke, K.F. O'Connell, W. Zachariae, E. Myers, and A.A. Hyman.(2011). Limiting amounts of centrosome material set centrosome size in C. elegans embryos. *Curr Biol*. **21**:1259-1267.

Delattre, M., C. Canard, and P. Gonczy.(2006). Sequential protein recruitment in C. elegans centriole formation. *Curr Biol*. **16**:1844-1849.

Glotzer, M., A.W. Murray, and M.W. Kirschner.(1991). Cyclin is degraded by the ubiquitin pathway. *Nature*. **349**:132-138.

Guderian, G., J. Westendorf, A. Uldschmid, and E.A. Nigg.(2010). Plk4 trans-autophosphorylation regulates centriole number by controlling betaTrCP-mediated degradation. *J Cell Sci*. **123**:2163-2169.

He, J., W.C. Chao, Z. Zhang, J. Yang, N. Cronin, and D. Barford.(2013). Insights into degron recognition by APC/C coactivators from the structure of an Acm1-Cdh1 complex. *Mol Cell*. **50**:649-660.

Holland, A.J., W. Lan, S. Niessen, H. Hoover, and D.W. Cleveland.(2010). Polo-like kinase 4 kinase activity limits centrosome overduplication by autoregulating its own stability. *J Cell Biol*. **188**:191-198.

Kemp, C.A., M.H. Song, M.K. Addepalli, G. Hunter, and K. O'Connell.(2007). Suppressors of zyg-1 define regulators of centrosome duplication and nuclear association in Caenorhabditis elegans. *Genetics*. **176**:95-113.

Kemphues, K.J., M. Kusch, and N. Wolf.(1988). Maternal-effect lethal mutations on linkage group II of Caenorhabditis elegans. *Genetics*. **120**:977-986.

Klebba, J.E., D.W. Buster, A.L. Nguyen, S. Swatkoski, M. Gucek, N.M. Rusan, and G.C. Rogers.(2013). Polo-like kinase 4 autodestructs by generating its Slimb-binding phosphodegron. *Curr Biol*. **23**:2255-2261.

Lettman, M.M., Y.L. Wong, V. Viscardi, S. Niessen, S.H. Chen, A.K. Shiau, H. Zhou, A. Desai, and K. Oegema.(2013). Direct binding of SAS-6 to ZYG-1 recruits SAS-6 to the mother centriole for cartwheel assembly. *Dev Cell*. **25**:284-298.

Matsusaka, T., M. Enquist-Newman, D.O. Morgan, and J. Pines.(2014). Co-activator independent differences in how the metaphase and anaphase APC/C recognise the same substrate. *Biol Open*. **3**:904-912.

Medley, J.C., L.E. DeMeyer, M.M. Kabara, and M.H. Song.(2017a). APC/C(FZR-1) Controls SAS-5 Levels To Regulate Centrosome Duplication in Caenorhabditis elegans. *G3 (Bethesda)*. **7**:3937-3946.

Medley, J.C., M.M. Kabara, M.D. Stubenvoll, L.E. DeMeyer, and M.H. Song.(2017b). Casein kinase II is required for proper cell division and acts as a negative regulator of centrosome duplication in Caenorhabditis elegans embryos. *Biol Open*. **6**:17-28.

Meghini, F., T. Martins, X. Tait, K. Fujimitsu, H. Yamano, D.M. Glover, and Y. Kimata.(2016). Targeting of Fzr/Cdh1 for timely activation of the APC/C at the centrosome during mitotic exit. *Nat Commun*. **7**:12607.

Nakayama, K.I., and K. Nakayama.(2006). Ubiquitin ligases: cell-cycle control and cancer. *Nat Rev Cancer*. **6**:369-381.

Nigg, E.A., and A.J. Holland.(2018). Once and only once: mechanisms of centriole duplication and their deregulation in disease. *Nat Rev Mol Cell Biol*. **19**:297-312.

O'Connell, K.F., C. Caron, K.R. Kopish, D.D. Hurd, K.J. Kemphues, Y. Li, and J.G. White.(2001). The C. elegans zyg-1 gene encodes a regulator of centrosome duplication with distinct maternal and paternal roles in the embryo. *Cell*. **105**:547-558.

Paix, A., A. Folkmann, D. Rasoloson, and G. Seydoux.(2015). High Efficiency, Homology-Directed Genome Editing in Caenorhabditis elegans Using CRISPR-Cas9 Ribonucleoprotein Complexes. *Genetics*. **201**:47-54.

Peel, N., M. Dougherty, J. Goeres, Y. Liu, and K.F. O'Connell.(2012). The C. elegans F-box proteins LIN-23 and SEL-10 antagonize centrosome duplication by regulating ZYG-1 levels. *J Cell Sci*. **125**:3535-3544.

Pelletier, L., E. O'Toole, A. Schwager, A.A. Hyman, and T. Muller-Reichert.(2006). Centriole assembly in Caenorhabditis elegans. *Nature*. **444**:619-623.

Pfleger, C.M., and M.W. Kirschner.(2000). The KEN box: an APC recognition signal distinct from the D box targeted by Cdh1. *Genes Dev*. **14**:655-665.

Puklowski, A., Y. Homsi, D. Keller, M. May, S. Chauhan, U. Kossatz, V. Grunwald, S. Kubicka, A. Pich, M.P. Manns, I. Hoffmann, P. Gonczy, and N.P. Malek.(2011). The SCF-FBXW5 E3-ubiquitin ligase is regulated by PLK4 and targets HsSAS-6 to control centrosome duplication. *Nat Cell Biol*. **13**:1004-1009.

Rogers, G.C., N.M. Rusan, D.M. Roberts, M. Peifer, and S.L. Rogers.(2009). The SCF Slimb ubiquitin ligase regulates Plk4/Sak levels to block centriole reduplication. *J Cell Biol*. **184**:225-239.

Shimanovskaya, E., V. Viscardi, J. Lesigang, M.M. Lettman, R. Qiao, D.I. Svergun, A. Round, K. Oegema, and G. Dong.(2014). Structure of the C. elegans ZYG-1 cryptic polo box suggests a conserved mechanism for centriolar docking of Plk4 kinases. *Structure*. **22**:1090-1104.

Song, M.H., L. Aravind, T. Muller-Reichert, and K.F. O'Connell.(2008). The conserved protein SZY-20 opposes the Plk4-related kinase ZYG-1 to limit centrosome size. *Dev Cell*. **15**:901-912.

Song, M.H., Y. Liu, D.E. Anderson, W.J. Jahng, and K.F. O'Connell.(2011). Protein phosphatase 2A-SUR-6/B55 regulates centriole duplication in C. elegans by controlling the levels of centriole assembly factors. *Dev Cell*. **20**:563-571.

Strnad, P., S. Leidel, T. Vinogradova, U. Euteneuer, A. Khodjakov, and P. Gonczy.(2007). Regulated HsSAS-6 levels ensure formation of a single procentriole per centriole during the centrosome duplication cycle. *Dev Cell*. **13**:203-213.

Stubenvoll, M.D., J.C. Medley, M. Irwin, and M.H. Song.(2016). ATX-2, the C. elegans Ortholog of Human Ataxin-2, Regulates Centrosome Size and Microtubule Dynamics. *PLoS Genet*. **12**:e1006370.

Sugioka, K., D.R. Hamill, J.B. Lowry, M.E. McNeely, M. Enrick, A.C. Richter, L.E. Kiebler, J.R. Priess, and B. Bowerman.(2017). Centriolar SAS-7 acts upstream of SPD-2 to regulate centriole assembly and pericentriolar material formation. *Elife*. **6**.

Tang, C.J., R.H. Fu, K.S. Wu, W.B. Hsu, and T.K. Tang.(2009). CPAP is a cell-cycle regulated protein that controls centriole length. *Nat Cell Biol*. **11**:825-831.

Table 1. Genetic Analysis

Strain	°C	% Embryonic Viability (ave ± sd)	n (Progeny)
wild-type (N2)		99.9 ± 0.3	719
ZYG-1:DB1(1A)		99.5 ± 1.4	1873
ZYG-1:DB2(2A)		99.9 ± 0.3	2181
ZYG-1:DB3(2A)		99.8 ± 0.4	2174
ZYG-1:DB4(1A)		99.3 ± 1.7	1528
SAS-5:KEN(3A)		99.8 ± 0.6	2202
fzr-1(bs31)		99.8 ± 0.9	1087
zyg-1(it25)	22.5	14.0 ± 11.8	1953
zyg-1(it25): ZYG-1:DB1(1A)		0.1 ± 0.5	2072
zyg-1(it25): ZYG-1:DB2(2A)		0.1 ± 0.9	2042
zyg-1(it25): ZYG-1:DB3(2A)		85.2 ± 13.6	3959
zyg-1(it25): ZYG-1:DB4(1A)		0.0 ± 0.0	2295
zyg-1(it25): ZYG-1:DB2(2A); SAS-5:KEN(3A)		6.10 ± 5.1	1840
zyg-1(it25): ZYG-1:DB3(2A); SAS-5:KEN(3A)		81.4 ± 13.2	3882
zyg-1(it25); SAS-5:KEN(3A)		59.5 ± 18.1	4006
zyg-1(it25) fzr-1(bs31)		99.1 ± 2.4	1451
zyg-1(it25)		5.4 ± 6.3	2325
zyg-1(it25): ZYG-1:SB(S335A)		16.5 ± 12.5	1874
zyg-1(it25): ZYG-1:SB(T339A)		15.4 ± 12.2	2177
zyg-1(it25): ZYG-1:SB(2A)	22.5	58.8 ± 12.1	2401
zyg-1(it25): ZYG-1:DB3(2A)		45.7 ± 9.7	2639
zyg-1(it25): ZYG-1:SB+DB3(4A)		78.9 ± 9.5	3373
zyg-1(it25) fzr-1(bs31)		99.5 ± 1.9	1444
zyg-1(it25)		0.0 ± 0.0	880
zyg-1(it25): ZYG-1:SB(S335A)		0.8 ± 1.9	536
zyg-1(it25): ZYG-1:SB(T339A)		1.1 ± 1.9	547
zyg-1(it25): ZYG-1:SB(2A)	23	19.6 ± 9.6	395
zyg-1(it25): ZYG-1:DB3(2A)		20.5 ± 12.5	379
zyg-1(it25): ZYG-1:SB+DB3(4A)		47.3 ± 26.0	566
zyg-1(it25) fzr-1(bs31)		94.3 ± 12.0	718
zyg-1(it25)		0.0 ± 0.0	1010
zyg-1(it25): ZYG-1:SB(S335A)		0.0 ± 0.0	789
zyg-1(it25): ZYG-1:SB(T339A)		0.0 ± 0.0	741
zyg-1(it25): ZYG-1:SB(2A)	24	1.6 ± 3.3	682
zyg-1(it25): ZYG-1:DB3(2A)		1.5 ± 2.4	497
zyg-1(it25): ZYG-1:SB+DB3(4A)		4.3 ± 3.4	627
zyg-1(it25) fzr-1(bs31)		64.4 ± 15.5	830
zyg-1(it25)		0.0 ± 0.0	708
zyg-1(it25): ZYG-1:SB(2A)		0.0 ± 0.0	627
zyg-1(it25): ZYG-1:DB3(2A)	25	0.0 ± 0.0	747
zyg-1(it25): ZYG-1:SB+DB3(4A)		0.0 ± 0.0	685
zyg-1(it25) fzr-1(bs31)		2.4 ± 1.7	645

Figures (1-3)

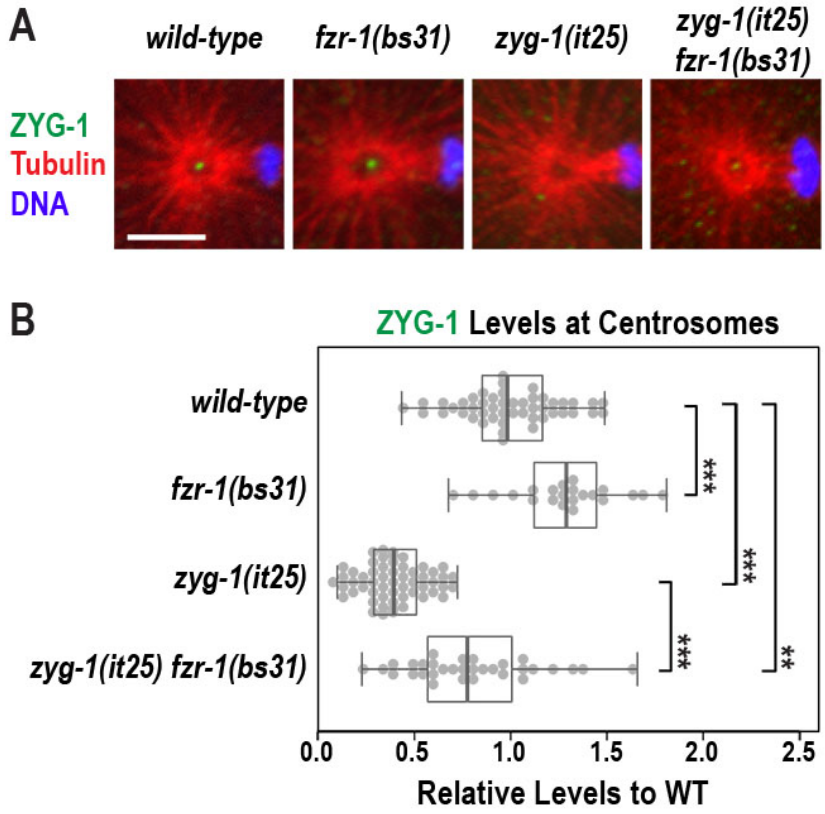

Figure 1. Loss of FZR-1 results in elevated ZYG-1 levels at centrosomes. (A) Images of anterior centrosomes stained for ZYG-1 at the first anaphase embryo. Bar, 5 μm. (B) Quantification of centrosomal ZYG-1 levels at the first anaphase. Each dot represents a centrosome.

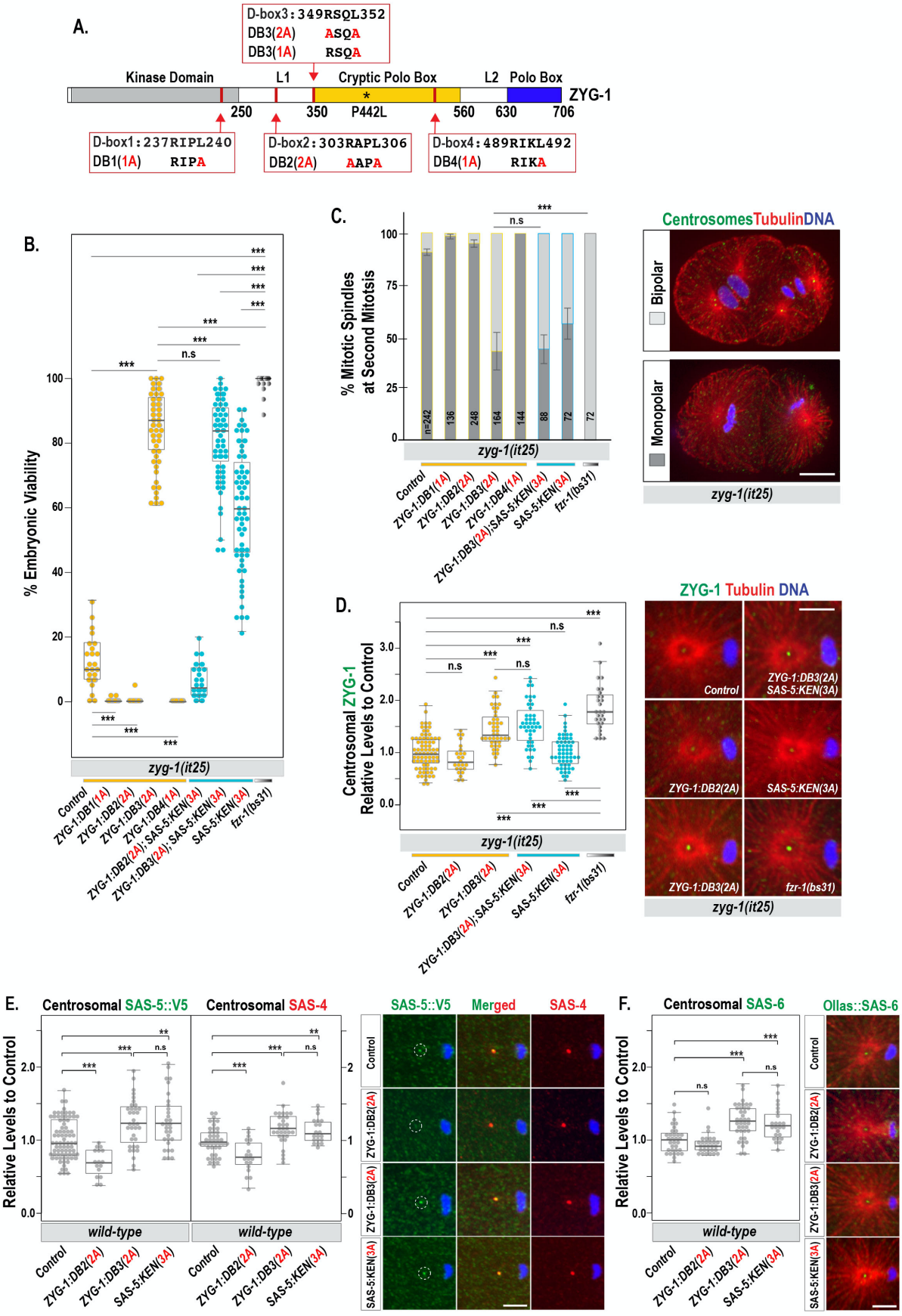

Figure 2. Mutating ZYG-1 D-box3 motif leads to *zyg-1* suppression and elevated centrosomal ZYG-1 levels. (A) ZYG-1 protein structure illustrates the location of D-box motifs and alanine substitutions, and functional domains. (B) Embryonic viability at 22.5°C (see **Table 1**). Each dot represents a hermaphrodite. (C) Quantification of mitotic spindles in two-cell embryos at 23°C. Average and standard deviation (SD) are presented. n is the number of blastomeres (left). Embryos are stained for centrosomes (ZYG-1), microtubules and DNA, illustrating mitotic spindles at the second mitosis. Bar, 10 μm (right). (D) Quantification of centrosome-associated ZYG-1 levels at the first anaphase (left). Centrosomes are stained for ZYG-1 (green) at the first anaphase. Bar, 5 μm (right). (E,F) Quantification of centrosomal levels of SAS-5 (E), SAS-4 (E), and SAS-6 (F) at the first anaphase. (D-F) Each dot represents a centrosome; Anterior centrosomes are presented. Bar, 5 μm.

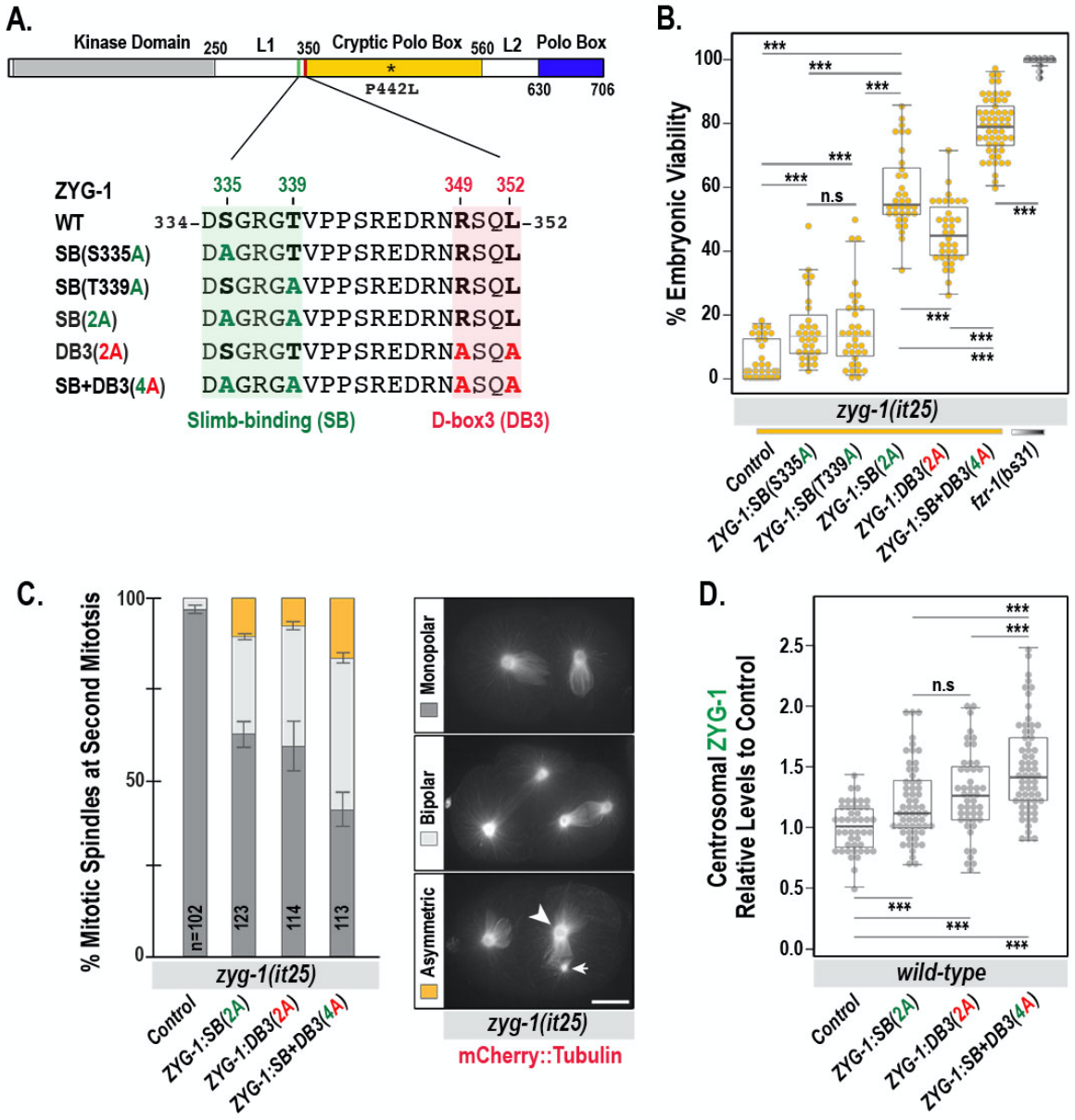

Figure 3. APC/C^{FZR-1} and SCF$^{Slimb/\beta TrCP}$ regulate ZYG-1 levels cooperatively (A) ZYG-1 protein structure illustrates the locations of D-box and Slimb-binding motifs and alanine substitutions. (B) Embryonic viability at 22.5°C (see Table 1). Each dot represents a hermaphrodite. (C) Quantification of mitotic spindles in two-cell embryos expressing mCherry::Tubulin at 24°C. Arrow and arrowhead indicate asymmetric centrosomes in a blastomere. Bar, 10 μm. n is the number of blastomeres. Average and SD are presented. (D) Quantification of centrosomal ZYG-1 levels at the first anaphase. Each dot represents a centrosome.